Frame Synchronization Algorithms for Satellite Internet of Things Scenarios

Marco Liess*, Francisco Lázaro†, Andrea Munari†
*Chair of Integrated Systems, Technical University of Munich
Munich, Germany. Email: marco.liess@tum.de
†Institute of Communications and Navigation of DLR (German Aerospace Center),
Wessling, Germany. Email: {Francisco.LazaroBlasco, Andrea.Munari}@dlr.de

***Abstract*—Non-terrestrial networks (NTNs) such as satellite constellations offer a large coverage area and the potential to serve vast populations of devices, and they are hence a promising solution for multiple Internet of Things (IoT) applications. Given the power constraints of typical IoT devices, low earth orbit (LEO) satellites have to be considered due to the improved link budget. A common characteristic of such satellite links is a large Doppler shift, which introduces additional challenges to the problem of frame synchronization. In this work we consider several frame synchronization algorithms, comparing their robustness against frequency offsets in different scenarios. The main finding of this paper is that a commonly considered algorithm, which is derived as a low-complexity approximation of the optimal likelihood-ratio test, exhibits a poor performance for low signal-to-noise ratio (SNR) values typical of satellite scenarios. In such realistic scenarios, a technique known as bank of correlators reaches the best performance among the considered algorithms but has a very high complexity. An FFT based technique commonly known as swiveled correlation seems to provide the best tradeoff between performance and complexity.**

I. Introduction

The Internet of Things (IoT) has become a fundamental technology for many next-generation networking applications, driven by a growing amount of research and industrial interest. Such applications include environmental monitoring and asset tracking, as well as smart homes and factories, where devices with sensors and actuators are interconnected to monitor, supervise and control specific tasks. At a high level of abstraction, the IoT aims at interconnecting vast numbers of terminals, which are often constrained in power and complexity. To enable this communications model, several commercial solutions have been developed in the terrestrial domain, epitomized by LoRa [1] and SigFox [2]. On the other hand, the past few years have witnessed an increased attention towards the use of non-terrestrial networks (NTNs), leveraging on constellations of low earth orbit (LEO) satellites to provide IoT connectivity over wide coverage areas in a cost-effective manner. This is also emphasized by recent 3GPP releases about the standardization of narrowband IoT (NB-IoT) for NTNs, e.g. [3].

Although this provides a promising solution from an architectural point of view, the nature of a satellite link with IoT terminals poses new challenges that span all the layers of the protocol stack. Among them, packet detection plays an important role. Indeed, due to power limitations, most IoT devices may be in sleep mode for most of the time and only sporadically generate traffic in the form of short packets. At the receiver, incoming messages have to be efficiently detected, so as to trigger the decoding chain only when needed. This task is commonly known as frame synchronization for bursty transmissions or "one shot" frame synchronization [4], and it is a challenging task in (LEO) satellite-based IoT systems due to the severe power constraints of the transmitting devices and the large Doppler shifts experienced.

One possible strategy to tackle this problem is to pre-compensate for the expected frequency shift at the transmitter, as envisioned in the 3GPP [3]. However, to compute the expected Doppler shift, an accurate knowledge of the terminals position and the satellite orbit, as well as a stable time reference and large enough computational resources are required. As these requirements may not all be fulfilled for typical IoT devices, the Doppler shift has to be dealt with when performing frame synchronization at the receiver.

Frame synchronization algorithms typically rely on a likelihood function $L(\mu)$, that measures the probability that the start of the frame is located at time μ. In this work, we consider preamble-based frame synchronization, where a known sequence of symbols is prepended to every packet to assist synchronization. Hence, one could say that the goal of the likelihood function is to only provide a large output when presented with the preamble. To interpret the output of the likelihood function and decide whether a packet was detected, mainly two strategies have been used: maximum likelihood and hypothesis testing. The essence of the former method is to examine a window of P symbols, where P is typically equal to the length of one frame, and select the time position $\hat{\mu}$ which maximizes the likelihood function as the one at which the preamble start can be found. The latter method compares the output of the likelihood function to an adjustable threshold for every sample, and declares the potential presence of a preamble whenever the threshold is exceeded. In this work, we consider only hypothesis testing, since it is more in accordance with the unpredictable nature of IoT transmissions.

Several works in literature have considered the problem of frame synchronization with a frequency offset using hypothesis testing. One line of research considers deriving

an optimal test and approximating it with a low-complexity expression [5], [6], [7], [8]. Other works follow an algorithmic approach [9], [10], [11], [12], building up on correlation techniques, which are known to be the optimal solution to the maximum likelihood frame synchronization problem without carrier frequency uncertainty [4]. The simulations provided in these works mostly focus on moderate SNRs of around $E_S/N_0 \approx 0\,\mathrm{dB}$.

The mentioned problem is rather well-studied in literature for conventional communication systems, however, the particular characteristics of novel satellite IoT scenarios require a reassessment in the context of satellite IoT. We contribute to the existing research mainly in two ways. First, we present results that indicate that whereas for a moderate SNR the schemes based on approximation of the optimal test perform close to optimally, their performance degrades strongly in the low SNR settings typical for satellite IoT applications. Second, we include the effects of intersymbol interference (ISI) due to imperfect receive filtering on the detection algorithms. These two aspects are relevant for a satellite IoT setting, and, as we will show in this paper, they have a strong practical impact.

II. Simplified Baseband Setting

In the first part of this paper, we focus on a simplified signal model for which it is possible to derive an upper bound on the performance of any frame synchronization scheme.

In particular, following [7], we consider the transmission of a packet consisting only of a preamble $c[k]$, which is an M-ary phase-shift keying (PSK) modulated symbol sequence of length K. Furthermore, we assume that the signal is transmitted over an additive white Gaussian noise (AWGN) channel and that it is affected by a Doppler shift F_d and an initial phase offset ϕ. Thus, the received signal can be expressed as

$$r[k] = c[k]\, e^{j(\theta k+\phi)} + n[k], \quad k \in \{0, K-1\}.$$

Hereby, $\theta = 2\pi f_d = 2\pi F_d T_S$ is the Doppler shift normalized to the symbol rate in radians/sample, T_S is the symbol period, $n[k]$ is zero-mean complex white Gaussian noise with a variance of $\sigma_n^2 = N_0/2$ in each dimension, and k is the time index. We shall assume that the phase shift ϕ is uniformly distributed on $[-\pi, \pi]$ and that the Doppler shift is also uniformly distributed on $[-f_{\max}, f_{\max}]$.

Casting the detection problem as a hypothesis testing problem, we define the following two hypotheses:

$$\mathcal{H}_0 : r[k] = n[k],$$
$$\mathcal{H}_1 : r[k] = c[k]\, e^{j(\theta k+\phi)} + n[k].$$

The null hypothesis $\mathcal{H}_0$ describes the case in which the incoming signal does not contain the preamble and is only defined by noise. The alternative hypothesis $\mathcal{H}_1$ accounts for the cases in which the signal contains the Doppler affected preamble and therefore stands for the location of the start of the packet. Following [7], [13], [14], we focus on distinguishing between $\mathcal{H}_0$ and $\mathcal{H}_1$, thereby ignoring all those cases in which the preamble is only partly contained in the received signal. As explained in [13], this simplification is well justified provided that the chosen preamble has good autocorrelation properties.

To decide between the two hypotheses, the Neyman-Pearson (NP) lemma [15] states that the most powerful test, i.e., the optimal decision rule, is given by a likelihood-ratio test (LRT), where the ratio of the probability density functions (PDFs) of the two hypotheses are compared to a threshold λ. If the ratio stays below the threshold the null-hypothesis $\mathcal{H}_0$ is accepted, whereas $\mathcal{H}_1$ is accepted if the threshold is exceeded. The likelihood function corresponding to the optimal LRT can be formulated as

$$L_{\mathrm{O}}(\mu) = \frac{f_{\mathbf{R}}(\mathbf{r}|\mathcal{H}_1)}{f_{\mathbf{R}}(\mathbf{r}|\mathcal{H}_0)} \underset{\mathcal{H}_0}{\overset{\mathcal{H}_1}{\gtrless}} \lambda,$$

where $\mathbf{r} = (r[\mu+0], r[\mu+1], ..., r[\mu+K-1])$ is the vector of incoming samples, and $\mathbf{R} = (R[\mu+0], R[\mu+1], ..., R[\mu+K-1])$ is its associated random variable.

For the simplified environment assumed in this section, it is actually possible to find a closed form expression for the optimal LRT, see [7] and [16]:

$$L_{\mathrm{O}}(\mu) = \int_{-2\pi f_{\max}}^{2\pi f_{\max}} I_0\left(\frac{2}{\sigma_n^2}\left|\sum_{k=0}^{K-1} r[\mu+k]\, c^*[k]\, e^{-j\theta k}\right|\right) d\theta \underset{\mathcal{H}_0}{\overset{\mathcal{H}_1}{\gtrless}} \lambda, \tag{1}$$

where $I_0(x)$ is the modified Bessel function of the first kind and zeroth order, [17]:

$$I_0(x) = \frac{1}{2\pi}\int_{-\pi}^{\pi} e^{x\cos(\phi)}\, d\phi.$$

Eq. (1) serves as an upper bound on the problem of frame synchronization in the given setting, although it cannot be implemented in practice (see [16] for details).

III. Detectors

In this section, we present several detection schemes, which in contrast to the optimal LRT presented in the previous section, have low complexity and thus offer practical implementations.

A. Approximation of the Optimal LRT

A straightforward approach to finding a lower complexity detector with good performance is to approximate the optimal LRT by replacing the Bessel function with a low complexity Taylor polynomial [5], [6], [7]. In particular, if one approximates it by x^4 and sets the maximum Doppler shift to $f_{\max} = 0.5$, the likelihood function simplifies to [7], [16]:

$$L_{\mathrm{A}}(\mu) = \sum_{m=1}^{K-1}\left|\sum_{k=m}^{K-1} r^*[\mu+k]\, c[k]\, r[\mu+k-m]\, c^*[k-m]\right|^2.$$

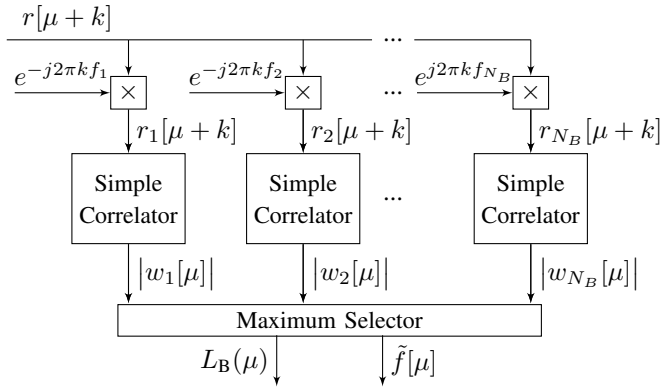

Fig. 1. Block diagram of the bank of correlators. Each branch is shifted by a different frequency $f_i = f_{\max} - (i-1)\Delta f$, where i is the index of the branch.

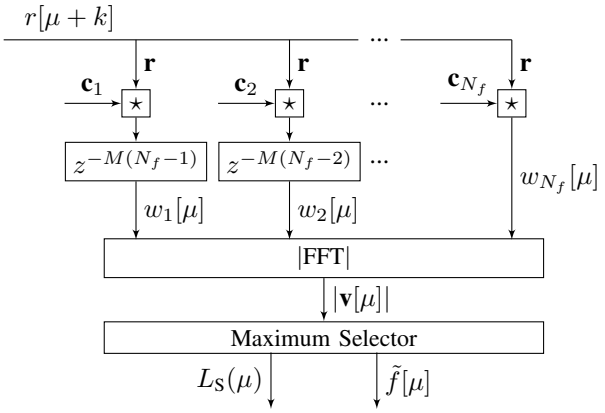

Fig. 2. Block diagram of the swiveled correlator.

B. Simple Correlator

The simple correlator, which is widely used in practice, simply computes the correlation between the incoming sample stream and the preamble. Relying on good autocorrelation properties of the preamble, the receiver can detect the start of the frame by the peak in the correlation. The corresponding likelihood function is given by

$$L_{\mathrm{C}}(\mu) = \left| \sum_{k=0}^{K-1} r[\mu+k]\, c^*[k] \right|.$$

Despite its simplicity, the simple correlator is very robust against noise for long preambles. However, its performance quickly degrades when a Doppler shift is present, which is elaborated in the Appendix.

C. Bank of Correlators

The bank of correlators aims at improving the detection performance for large Doppler shifts by operating multiple simple correlators at different center frequencies, see Fig. 1. Hereby, the number of parallel correlators N_B, or branches, can be varied according to the requirements of the system. This is reflected in the resolution of the bank of correlators, which describes the frequency difference between two branches and is given as

$$\Delta f = 2\frac{f_{\max}}{N_B - 1}.$$

Its likelihood function is given by

$$L_{\mathrm{B}}(\mu) = \max_i \left(\left| \sum_{k=0}^{K-1} e^{-j2\pi k (f_{\max} - (i-1)\Delta f)}\, r[\mu+k]\, c^*[k] \right| \right),$$

where $i \in \{1, N_B\}$.

The main idea of the algorithm is to differently shift the frequency of the input signal in order to counteract the Doppler shift in one of the branches. In the correct branch, i.e., the branch corresponding to the frequency shift closest to the actual Doppler shift, the remaining residual frequency offset f_r is expected to only have a minor influence on the output of the succeeding correlation. To ensure this behaviour, the maximum residual frequency offset $\hat{f}_r$ in the correct branch can be controlled by the number of parallel correlators, as it is directly proportional to the resolution of the bank of correlators, i.e., $\hat{f}_r = \Delta f/2$. Thereby, an arbitrary small maximum residual frequency offset could be guaranteed by choosing a very large number of branches, effectively resulting in a Doppler-free scenario. This, however, results in an increased complexity, see Section VI. One of the advantages of this technique is that it can provide a (coarse) frequency estimate $\tilde{f}$ at its output. In particular, the frequency estimate corresponds to the center frequency of the branch which produced the largest output.

D. Swiveled Correlator

The swiveled correlator was first presented in [9] and it is practically used in the S-MIM system [18]. Its performance, neglecting ISI, was analyzed in [10]. In the swiveled correlator, the preamble is first split into N_f segments of length $M = K/N_f$ symbols, where we assume that K is divisible by N_f. Hence, the n-th preamble segment $\boldsymbol{c}_n$, $n \in \{1, N_f\}$, is given by

$$\boldsymbol{c}_n = (c[(n-1)M],\, c[(n-1)M+1], ...,\, c[nM-1]).$$

As it can be observed in Fig. 2, the swiveled correlator processes the signal on N_f parallel branches, where each branch is associated to a different preamble segment $\boldsymbol{c}_n$. The incoming signal $\boldsymbol{r}$ is then correlated with the respective preamble segment in each branch. The correlator outputs are then aligned in time by means of a delay. In particular, the n-th branch is delayed by $M(N_f - n)$ symbols and then used as input to a fast Fourier transform (FFT) block. Finally, the detection metric is obtained by taking the maximum among the N_S outputs of the FFT block. Intuitively, the FFT block is an efficient way of finding the frequency shift which results in a constructive addition of the signals in the N_f branches.

The FFT block generates N_S outputs, each of them associated to a discrete frequency, or frequency bin. If the Doppler frequency falls between two frequency bins, the

energy is shared and the amplitude in both bins is much lower than in the case of a frequency match. This reduces the potential to detect a peak in one of the output bins. In literature, this is also referred to as scalloping loss [19]. A common method to counter this issue is to employ zero-padding, i.e., extending the input to the FFT with Z zeros, which effectively adds more bins in the same frequency range, resulting in a total of $N_S = N_f + Z$ output bins.

The likelihood function of the swiveled correlator with zero-padding is given by

$$L_{\mathrm{S}}(\mu) = \max_{i \in \mathcal{I}} \left(\left| \sum_{n=1}^{N_f} \sum_{k=(n-1)M}^{nM-1} r[\mu+k]\, c^*[k]\, e^{-j2\pi \frac{n}{N_f+Z} i} \right| \right),$$

where $\mathcal{I}$ is the set of possible frequency bins, i.e., those that satisfy $|-0.5 + i/(N_f+Z)| \leq f_{\max}$. Similarly to the bank of correlators, the swiveled correlator also provides a (coarse) estimate of the frequency shift at its output, which simply corresponds to the frequency associated to the bin which yields the maximum output.

Let us now analyze the algorithm more closely by assuming that the preamble is fully contained in the input signal. In particular, let us assume that a preamble starts at sample $\mu = 0$. The correlation output in the n-th branch can be expressed as:

$$\begin{aligned} w_n[0] &= \sum_{k=(n-1)M}^{nM-1} e^{j(2\pi k f_d + \phi)}\, c[k]\, c^*[k] + \sum_{k=(n-1)M}^{nM-1} n[k]\, c^*[k] \\ &= e^{j2\pi f_d (n-1)M} \sum_{k=0}^{M-1} e^{j(2\pi k f_d + \phi)} + \sum_{k=(n-1)M}^{nM-1} n[k]\, c^*[k]. \end{aligned}$$

Hereby, we can observe that the Doppler induced phase difference between the output of adjacent branches w_n and w_{n+1} is $e^{j2\pi f_d M}$. Thus, we will only be able to unequivocally detect normalized frequency shifts in the range $f_d \in (-1/2M, 1/2M]$. To optimally cope with the Doppler shift, for the remainder of this work we choose $M = 1$.

IV. Simulations in the Simplified Baseband Setting

In this section, we compare the performance of the different detection algorithms in two different settings.

First we consider a *moderate* SNR setting with $E_S/N_0 = 0\,\mathrm{dB}$, a maximum Doppler shift $f_{\max} = 0.5$ and a preamble length of $K = 15$ symbols. Fig. 3 plots the simulation results of the receiver operating characteristic (ROC) for the different detectors and the upper bound. The curves show that the performance of the lower complexity detectors almost reach the upper bound, which is given by the optimal LRT in this setting.

The second setting considers parameters that are typical for satellite-based IoT applications. In particular, we consider an SNR of $E_S/N_0 = -9\,\mathrm{dB}$ and a preamble length of $K = 150$ symbols. The simulation results are given in Fig. 4. It can be observed how the bank of correlators L_{B} and the swiveled correlator L_{S} show close to optimal performance. However, the approximation of the optimal LRT L_{A} significantly drops

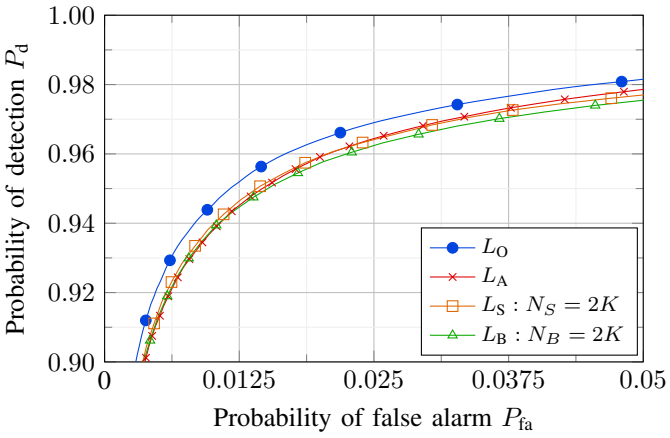

Fig. 3. Simulated ROC at $\frac{E_S}{N_0} = 0\,\mathrm{dB}$ for a preamble length $K = 15$ and maximum Doppler shift $f_{\max} = 0.5$.

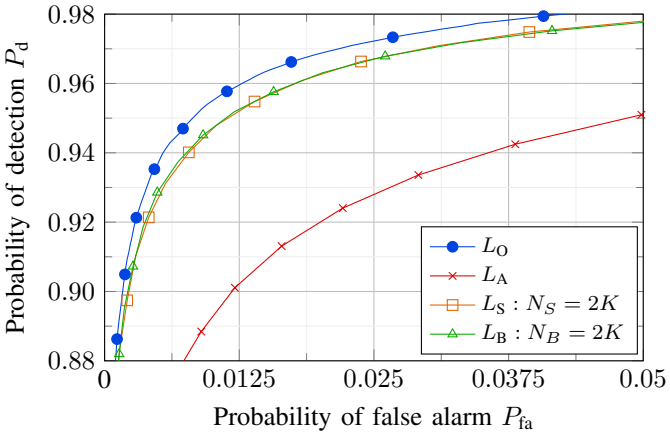

Fig. 4. Simulated ROC at $\frac{E_S}{N_0} = -9\,\mathrm{dB}$ for a preamble length $K = 150$ and maximum Doppler shift $f_{\max} = 0.5$.

in performance compared to the moderate SNR scenario. We speculate that this performance degradation, which had not yet been observed in literature, can be attributed to the approximation of the Bessel function, and leave a detailed analysis for further investigation.

Since a Doppler shift of $f_{\max} = 0.5$ can be considered very extreme, we provide further simulation results for a smaller Doppler range with $f_{\max} = 0.2$ and a preamble length of $K = 130$ in Fig. 5. The results show that the bank of correlators and the swiveled correlator again reach close to optimal performance, while the approximation of the optimal test performs poorly.

V. Simulations in a Realistic Satellite Setting

A. Signal Model

In the simplified baseband setting in Section II several processing steps were omitted, which have to be considered in a practical communication system. In particular, the modulated

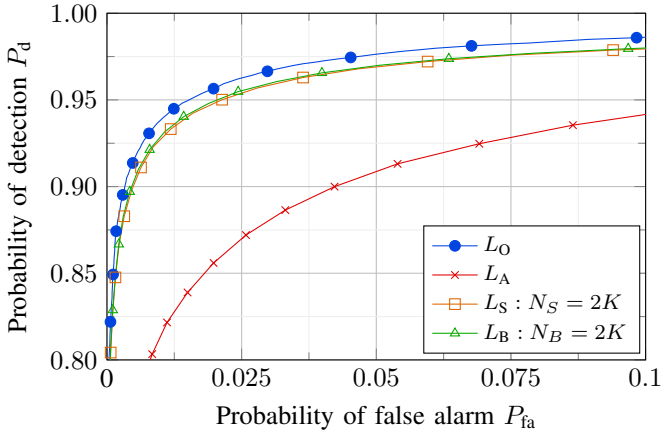

Fig. 5. Simulated ROC at $\frac{E_S}{N_0} = -9\,\mathrm{dB}$ for a preamble length $K = 130$ and maximum Doppler shift $f_\mathrm{max} = 0.2$.

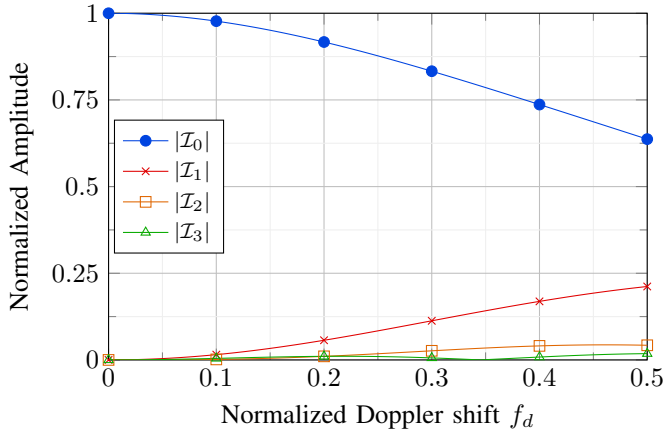

Fig. 6. $\mathcal{I}_n(f_d)$, $n = 0, 1, 2, 3$, as a function of the normalized Doppler shift f_d, for a SRRC matched filter pair with roll-off $\beta = 0.5$.

sequence has to undergo pulse shaping in order to generate a (bandlimited) waveform, which is then upconverted to carrier frequency and transmitted by an antenna. For the sake of simplicity, we assume that the channel applies a Doppler shift to the transmitted signal, as well as an attenuation and the addition of white Gaussian noise. After travelling through the channel, the signal is downconverted at the receiver. Hereby, the Doppler shift will remain as residual frequency offset in the downconverted signal. At this point, the signal can be expressed as

$$r(t) = \sum_{m=0}^{K-1} c[m]\, p(t - mT_S)\, e^{j\left(2\pi f_d \frac{t}{T_S} + \phi\right)} + \nu(t),$$

where $p(t)$ is the impulse response of the pulse shaping filter and the noise $\nu(t)$ has a constant power spectral density (PSD) of $N_0/2$.

In order to fulfill the Nyquist criterion and ensure ISI-free transmission, the received signal is then filtered using a matched receive filter. However, at the time of receive filtering, the Doppler shift of the incoming signal is unknown, and thus receive filtering introduces ISI.

The receive filtered signal can be represented as [20]:

$$z[k] = \Big(c[k]\mathcal{I}_0(f_d) + \sum_{\substack{m=0 \\ m\neq k}}^{K-1} c[m]\mathcal{I}_{k-m}(f_d)\Big) e^{j(2\pi k f_d + \phi)} + n[k],$$

where

$$\mathcal{I}_n(f_d) = \int_{-\infty}^{\infty} G(f + \frac{f_d}{T_S})\, P(f)\, e^{j2\pi f n T_S}\, df.$$

Hereby, $P(f)$ is the frequency response of the pulse shaping filter and $G(f + f_d/T_S)$ is the frequency response of the receive filter, shifted in frequency. The terms $\mathcal{I}_n(f_d)$ account for the ISI due to the Doppler shift f_d. In particular, $\mathcal{I}_0(f_d)$ represents the amplitude of the target symbol, while $\mathcal{I}_n(f_d)$ for $n \neq 0$ corresponds to the amplitude of the n-th adjacent symbol.

The terms $\mathcal{I}_0$, $\mathcal{I}_1$, $\mathcal{I}_2$ and $\mathcal{I}_3$ are plotted in Fig. 6 as a function of the normalized Doppler shift f_d, for a matched filter pair of square-root raised cosine (SRRC) pulses with a roll-off factor of $\beta = 0.5$. We can observe how for small Doppler shifts the effect of ISI is negligible since we have $\mathcal{I}_0 \simeq 1$ and $\mathcal{I}_n \simeq 0$, for $n > 0$. However, as the Doppler shift increases the ISI becomes stronger. Regarding the impact of the roll-off factor, as one could expect, the lower the roll-off factor, the stronger the ISI ($\mathcal{I}_i$, $i \geq 1$), and the weaker the amplitude of the target symbol ($\mathcal{I}_0$) across the range of Doppler shifts, resulting in an even quicker decline of signal quality for a growing Doppler shift.

From this discussion, it is obvious that the appearance of ISI will negatively impact the performance of any frame detection algorithm which is applied after (imperfect) receive filtering. However, for the bank of correlators, it is actually possible to avoid this problem. In particular, since each of the branches of the bank of correlators is processed independently, it is possible to apply receive filtering in each branch after the initial frequency shifting. This strategy, which unfortunately cannot be applied to any of the other detection algorithms, results in a slight increase in complexity, but can effectively mitigate ISI, provided that a sufficient number of branches is used.

B. Results

We consider a setting in which a LEO satellite at an altitude of 575 km services an area corresponding to a maximum slant range of 1300 km. The symbol rate is set to 250 kHz at a carrier frequency of 2 GHz. We expect the SNR to amount to -6 dB at the center of coverage and -13 dB at the edge of coverage. Pulse-shaping and receive filtering is performed with SRRC filters with a roll-off factor of 0.22. We consider a preamble length of $K = 350$ symbols. The simulation parameters are summarized in Table I.

TABLE I
PARAMETERS OF THE CONSIDERED LEO SATELLITE LINK

Description	Symbol	Value
Carrier frequency	f_c	2 GHz
Symbol rate	$\frac{1}{T_S}$	250 kHz
Satellite altitude	h	575 km
Maximum slant range	$d_{\max}$	1300 km
SNR at CoC	$\frac{E_s}{N_0}\|_{\text{CoC}}$	-6 dB
SNR at EoC	$\frac{E_s}{N_0}\|_{\text{EoC}}$	-13 dB
SRRC roll-off factor	β	0.22

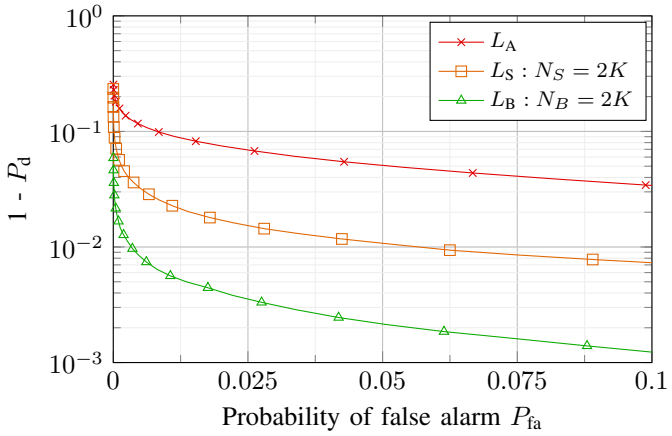

Fig. 7. Simulated ROC in realistic satellite setting following the parameters given in Table I for a preamble length $K = 350$.

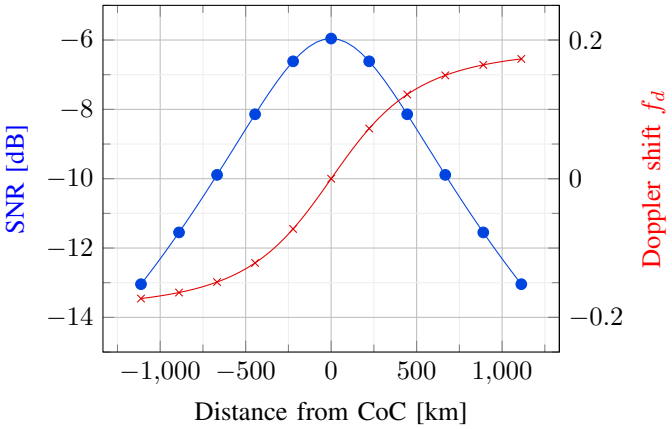

Fig. 8. SNR in dB and normalized Doppler shift f_d as a function of the distance from the center of coverage in km.

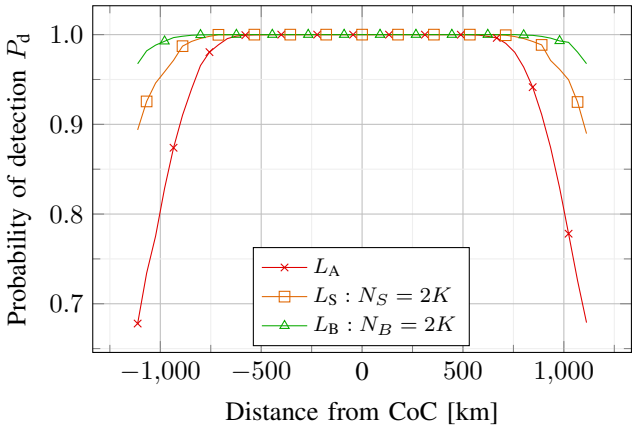

Fig. 9. Probability of detection P_{d} as a function of the distance from the center of coverage in km.

To simulate the transmission for any given terminal, we choose the terminal locations by uniformly sampling a point in the coverage area of the satellite, and then computing the corresponding Doppler shift and link budget. The results of the simulation are shown in Fig. 7. The approximation of the optimal LRT L_{A} again performs poorly, owing to the low SNR. The swiveled correlator shows a better performance, but it does not reach the performance of the bank of correlators, which performs best. The good performance of the bank of correlators can be attributed to the integration of a receive filter in each of its branches, which effectively mitigates ISI. In contrast, the approximation of the optimal LRT and the swiveled correlator operate with a single receive filter and suffer from ISI, which leads to a performance degradation.

The results shown in Fig. 7 are average results for the whole coverage area of the satellite. In the following, we have a closer look into the performance of the different detectors as a function of the exact terminal position within the coverage area. For illustration, we will place terminals on a line traversing the center of the coverage area in the direction of movement of the satellite. The presented discussion will also be indicative of the behaviour a terminal will experience when a satellite passes above it.

The resulting SNR and Doppler shift depending on the distance to the center of the coverage area are shown in Fig. 8, whereas Fig. 9 shows the probability of detection of the different schemes, assuming a fixed false alarm probability P_{fa} of 5%. It becomes apparent that, for all detectors, the performance is very good for points near the center of the coverage area, but degrades as the distance to the center increases, due to the increasing Doppler shift and decreasing SNR. However, this degradation is different for the different detectors. As expected, the degradation is strongest for the approximation of the optimal LRT, less severe for the swiveled correlator and the best performance with only a small degradation is achieved by the bank of correlators, which is only affected by the decreasing SNR, and not by the increasing Doppler shift due to the use of a receive filter on each branch.

VI. Computational Complexity

In this section, we analyze and compare the complexity of the different frame detection algorithms. In particular, we

TABLE II
COMPUTATIONAL COMPLEXITY OF THE DIFFERENT DETECTORS

Scheme	Operation Count	#Ops. for considered setting
L_{C}	$2L'+2K+2$	716
L_{B}	$N_B(2L'+2K+3)$	501,900
L_{S}	$2L'+2K-N_f-1$ $+4N_S(\log_2(N_S)+1)$	29,627
L_{A}	$2L'+2K^2+K-5$	245,359

provide a count of the number of operations, and we define as one operation a complex multiplication, complex addition, or the computation of the square root. Furthermore, we shall assume that the receive filter is implemented as a finite impulse response filter of length L'. A similar analysis was carried out in [11], however without considering receive filtering and assuming a suboptimal fixed configuration ($N_S = N_f = K$) for the swiveled correlator.

The operation counts were derived as follows. The simple correlator L_{C} first carries out receive filtering, corresponding to L' multiplications and $L'-1$ additions, and then computes the correlation with the length K preamble, which requires K multiplications, $K-1$ additions and 4 additional operations to compute the absolute value ($|z| = \sqrt{x^2+y^2}$, for $z = x+iy$). This yields a total of $2L'+2K+2$ operations.

Similarly, the bank of correlators L_{B} simply consists of N_B simple correlators applied in parallel, and additionally needs one operation to shift the frequency of the input signal in each branch. This yields a total of $N_B(2L'+2K+3)$ operations.

The swiveled correlator first carries out receive filtering, which requires $2L'-1$ operations, and then computes N_f correlations of length $M = K/N_f$, which requires $2K - N_f$ operations. The subsequent FFT requires $4N_S \log_2(N_S)$ operations[1] and an additional $4N_S$ operations to compute the absolute value of each output. This yields a total of $2L'+2K-N_f+4N_S(\log_2(N_S)+1)-1$ operations.

Also for the approximation of the optimal LRT the first step is receive filtering, yielding $2L'-1$ operations. The likelihood function then consists of a double sum. The inner sum requires $3(K-m)$ multiplications and $K-m-1$ additions, and an additional 3 operations to compute the absolute square. The outer sum requires $K-2$ additions to add the results of the inner sum, thus the operation count is

$$2L'-1+K-2+\sum_{m=1}^{K-1} 4(K-m)+2 = 2L'+2K^2+K-5.$$

Table II summarizes the operation counts for the different schemes and provides the number of operations considering the parameters in Section V, i.e., $K = 350$ and $N_B = N_S = 2K$, and assuming an impulse response of length $L' = 7$ for the receive filter.

The operation counts presented in this section are not to be taken as an exact measure of complexity, since this will depend strongly on multiple practical aspects. Nevertheless, they do allow us to order the algorithms in terms of complexity, and to conclude that the swiveled correlator has much lower complexity than the bank of correlators and the approximation of the optimal LRT.

[1]We consider here the well-known Cooley-Tukey FFT implementation [21]

VII. DISCUSSION & CONCLUSION

In this paper we have considered different frame detection algorithms both in an idealized setting, which disregards receive filtering, and in a more realistic setting that considers also the ISI due to imperfect receive filtering. The two main findings of this paper are the following. The first is that although the approximation of the optimal LRT provides promising results in moderate SNR values, its performance at low SNR, which is the expected regime of operation in satellite-based IoT, is very poor. This was confirmed for the simplified and realistic settings. The second finding is that in a realistic satellite IoT setting, the swiveled correlator exhibits both good performance and low complexity, and is thus a promising solution, although its performance degrades for large Doppler shifts due to ISI.

Due to space limitations, some interesting aspects could not be analyzed in detail in this paper. A first one would be deriving strategies to better cope with very large Doppler shifts in the swiveled correlator. Here, one option could be operating multiple swiveled correlators in parallel (and centered at different frequencies). This would improve performance at the cost of some additional complexity. However, we expect such a solution to still be less complex than the bank of correlators.

A further interesting research direction is evaluating the performance of the different algorithms in a more complete setting, considering the transmission of preambles followed by modulated data symbols, as well as the presence of transmissions from multiple users. Another aspect that is left for further study is operating the detection algorithms on an oversampled waveform since timing synchronization can only take place after successful frame synchronization.

While we do expect the trends identified in this paper to hold in full-scale implementation both in terms of performance and complexity, some interesting new aspects may emerge, such as, for example, the possibility to dynamically adapt the detection threshold λ depending on the load of the channel.

APPENDIX
CORRELATION LOSS R_0

This appendix analyzes the effect of a Doppler shift on the output of a correlator. A similar analysis can be found in [22]. For simplicity, we consider a noiseless scenario, where the input signal only contains the frequency shifted preamble, i.e.

$$r[\mu+k] = c[k]\, e^{j(2\pi k f_d+\phi)}.$$

Thus, we have that the (absolute value of the) correlator output corresponds to:

$$|R_0(f_d)| = \left| \sum_{k=0}^{K-1} e^{j(2\pi k f_d+\phi)}\, c[k]\, c^*[k] \right|, \qquad (2)$$

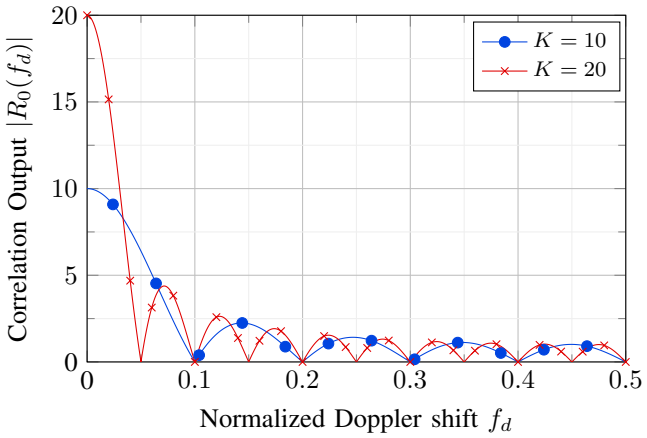

Fig. 10. Magnitude of $R_0(f_d)$ for different preamble lengths $K = 10$ and $K = 20$ in a noiseless scenario. Restricted to positive frequencies as function is symmetric.

Since we consider PSK modulation, we have $c[k]\,c^*[k] = E_S$. Choosing $E_S = 1$, without loss of generality, we can rewrite Eq. (2) as

$$|R_0(f_d)| = \left| \frac{\sin(K\pi f_d)}{\sin(\pi f_d)}\; e^{j((K-1)\pi f_d + \phi)} \right|.$$

This function is plotted for different preamble lengths in Fig. 10. It can be observed that the shape depends on the preamble length K. Hereby, mainly two characteristics can be established from the plot:

- For a normalized Doppler shift of $f_d = 0$, the amplitude of the output corresponds to the preamble length K. Therefore, longer preambles induce a larger correlation output and thus show an improved performance against noise.
- The amplitude of the output rapidly decreases for growing Doppler shifts. This effect depends on the preamble length. More precisely, we have that the longer the preamble, the more severe the degradation becomes.

Thus, we can conclude that in low SNR scenarios, where long preambles are needed to increase correlation output against the noise, the performance of the simple correlator will be very poor already for small Doppler shifts.

References

[1] LoRa Alliance, "The LoRa alliance wide area networks for Internet of Things," Accessed Dec. 6, 2021. [Online]. Available: https://www.lora-alliance.org

[2] Sigfox, "SIGFOX: The global communications service provider for the Internet of Things," Accessed Dec. 6, 2021. [Online]. Available: https://www.sigfox.com

[5] J. Gansman, M. Fitz, and J. Krogmeier, "Optimum and suboptimum frame synchronization for pilot-symbol-assisted modulation," *IEEE Transactions on Communications*, vol. 45, no. 10, pp. 1327–1337, 1997.

[3] 3GPP, "Study on narrow-band Internet of things (NB-IoT) /enhanced machine type communication (eMTC) support for non-terrestrial networks (NTN)," 3rd Generation Partnership Project (3GPP), Technical Report (TR) 36.763, 06 2021, version 17.0.0. [Online]. Available: https://www.3gpp.org/ftp/Specs/archive/36_series/36.763/

[4] J. Massey, "Optimum frame synchronization," *IEEE Transactions on Communications*, vol. 20, no. 2, pp. 115–119, 1972.

[6] Z. Y. Choi and Y. Lee, "Frame synchronization in the presence of frequency offset," *IEEE Transactions on Communications*, vol. 50, no. 7, pp. 1062–1065, 2002.

[7] R. Wuerll, J. Robert, G. Kilian, and G. Heuberger, "Optimal one-shot detection of preambles with frequency offset," in *2018 IEEE International Conference on Advanced Networks and Telecommunications Systems (ANTS)*, 2018, pp. 1–4.

[8] M. Chiani, "Noncoherent frame synchronization," *IEEE Transactions on Communications*, vol. 58, no. 5, pp. 1536–1545, 2010.

[9] M. Sust, R. Kaufmann, F. Molitor, and G. Bjornstrom, "Rapid acquisition concept for voice activated CDMA communication," in *[Proceedings] GLOBECOM '90: IEEE Global Telecommunications Conference and Exhibition*, 1990, pp. 1820–1826 vol.3.

[10] S. Spangenberg, I. Scott, M. Stephen, G. Povey, D. Cruickshank, and P. Grant, "An FFT-based approach for fast acquisition in spread spectrum communication systems," *Wireless Personal Communications*, vol. 13, pp. 27–55, 01 2000.

[11] R. Wuerll, J. Robert, G. Kilian, and A. Heuberger, "A comparison of methods for detecting preambles with frequency offset at low SNR," in *2017 2nd International Conference on Computer and Communication Systems (ICCCS)*, 2017, pp. 96–100.

[12] G. Corazza, R. Pedone, and M. Villanti, "Frame acquisition for continuous and discontinuous transmission in the forward link of satellite systems," *International Journal of Satellite Communications and Networking*, vol. 24, pp. 185 – 201, 03 2006.

[13] M. Chiani and M. Martini, "On sequential frame synchronization in AWGN channels," *IEEE Transactions on Communications*, vol. 54, no. 2, pp. 339–348, 2006.

[14] R. Pedone, M. Villanti, A. Vanelli-Coralli, G. E. Corazza, and P. T. Mathiopoulos, "Frame synchronization in frequency uncertainty," *IEEE Transactions on Communications*, vol. 58, no. 4, pp. 1235–1246, 2010.

[15] J. Neyman and E. S. Pearson, "On the problem of the most efficient tests of statistical hypotheses," *Philosophical Transactions of the Royal Society A*, vol. 231, pp. 289–337, 1933.

[16] M. Liess, "Frame synchronization for satellite-based Internet of Things (IoT) applications," Master's Thesis, Technische Universität München, Munich, Germany, Dec. 2021.

[17] G. N. Watson, *A treatise on the theory of Bessel functions*. Cambridge university press, 1995.

[18] R. De Gaudenzi, O. del Rio Herrero, and G. Gallinaro, "Enhanced spread ALOHA physical layer design and performance," *International Journal of Satellite Communications and Networking*, vol. 32, no. 6, pp. 457–473, 2014. [Online]. Available: https://onlinelibrary.wiley.com/doi/abs/10.1002/sat.1078

[19] F. Harris, "On the use of windows for harmonic analysis with the discrete fourier transform," *Proceedings of the IEEE*, vol. 66, no. 1, pp. 51–83, 1978.

[20] T. Pollet and M. Moeneclaey, "The effect of carrier frequency offset on the performance of band limited single carrier and OFDM signals," in *Proceedings of GLOBECOM'96. 1996 IEEE Global Telecommunications Conference*, vol. 1, 1996, pp. 719–723 vol.1.

[21] J. W. Cooley and J. W. Tukey, "An algorithm for the machine calculation of complex fourier series," *Mathematics of computation*, vol. 19, no. 90, pp. 297–301, 1965.

[22] R. Stirling-Gallacher, A. Hulbert, and G. J. Povey, "A fast acquisition technique for a direct sequence spread spectrum signal in the presence of a large Doppler shift," in *Proc. of Int. Symp. on Spread Spectrum Tech. and App., ISSSTA 95*, vol. 1. IEEE, Sep. 1996, pp. 156–160.